Water Budget of a Mesoscale Convective System in the Tropics[1]

JOHN F. GAMACHE AND ROBERT A. HOUZE, JR.

Department of Atmospheric Sciences, University of Washington, Seattle, WA 98195

(Manuscript received 8 November 1982, in final form 9 March 1983)

ABSTRACT

A squall-line cloud cluster observed in the Global Atmospheric Research Program's Atlantic Tropical Experiment (GATE) is studied as an example of a mesoscale convective system in the tropics. The system is divided into convective and stratiform regions. Composite wind, vertical motion, humidity, radar and satellite data fields have been derived for the system and are used to calculate the components of the water budgets of each region. Particular attention is devoted to understanding the sources of condensate for the stratiform region. The mesoscale updraft in the stratiform cloud accounts for 25–40% of the condensate making up the stratiform cloud, while the remaining 60–75% is supplied by horizontal transfer to the stratiform region of condensate generated in the cumulonimbus towers of the convective region.

1. Introduction

Most of the precipitation in the tropics, and in many mid-latitude locations during the warm season, falls in mesoscale convective systems which contain both deep convective and stratiform clouds and precipitation. A mesoscale convective system is typically identified in satellite imagery by a large cirrus shield (~200–1000 km). In the tropics these systems are referred to as *cloud clusters* (Martin and Suomi, 1972; Frank, 1970) and in the mid-latitudes as *mesoscale convective complexes* (Maddox, 1980). The structure of cloud clusters has been discussed in detail by Houze and Betts (1981) and Houze (1982), while Maddox (1981) has given a detailed description of the composite structure of mesoscale convective complexes. Houze and Hobbs (1982) have noted apparent similarities in the structures of cloud clusters and mesoscale convective complexes. To the extent that mesoscale convective systems are similar in the tropics and mid-latitudes, what is learned about either type of system will contribute to the general knowledge of mesoscale convective systems. In this study, a tropical cloud cluster is examined.

As a result of the observations and analyses of the Global Atmospheric Research Program's Atlantic Tropical Experiment (GATE) and Monsoon Experiment (MONEX), a conceptual model for a tropical cloud cluster has been developed. Houze and Betts (1981) discussed this model in detail and various aspects of its horizontal and vertical air motion field were confirmed by Gamache and Houze (1982; hereafter referred to as GH). A schematic of the model is shown in Fig. 1. The schematic can be interpreted as representing either the mature cluster or its time-averaged structure. The left portion of the schematic represents the portion of the cluster occupied by cumulonimbus clouds. This region is called the convective region. In the convective region, water and ice are condensed (C_u) in convective updrafts which carry warm moist high-θ_e air from the boundary layer to the upper troposphere. Much of the condensate (C_u) falls out of the updrafts and either evaporates (E_{cd}) in the nearly saturated convective downdrafts or reaches the surface as heavy convective rain (R_c). The rest of the condensate is eventually detrained from the updrafts. It then either evaporates into the environment of the cumulonimbi (E_{ce}) or is carried unevaporated (C_A) into the mesoscale stratiform cloud adjacent to the convection. The stratiform region is represented by the right-hand portion of the schematic shown in Fig. 1. Mesoscale quiescent ascent present within the stratiform cloud produces condensate (C_{mu}), which can either fall from the stratiform cloud or be advected out of the cloud cluster where it is evaporated in the environment (E_{me}). The condensate that falls from the stratiform cloud either reaches the surface as relatively light, steady stratiform rain (R_m) or evaporates (E_{md}) in unsaturated air in the mesoscale downdraft below. Concentrated melting of the precipitation occurs in a layer of air just below the 0°C level. Melting and evaporation cool the air and help to maintain the mesoscale downdraft.

Following Houze *et al.* (1980), we express the water budget depicted in Fig. 1 in two equations, one for the convective region,

[1] Contribution No. 658, Department of Atmospheric Sciences, University of Washington.

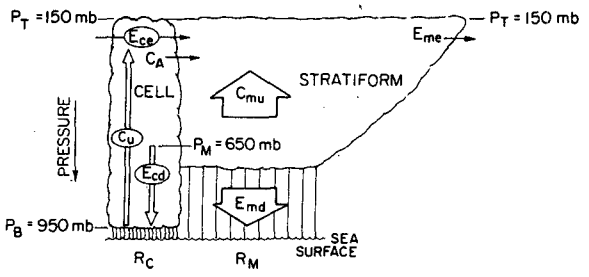

FIG. 1. Schematic diagram of the squall-system water budget. The squall-line and stratiform-cloud water budgets are depicted in the left and right portions, respectively, of the figure. The water budget parameters C_u, E_{cd}, E_{ce}, C_A, R_c, C_{mu}, E_{md}, E_{me} and R_m are defined and discussed in Section 1 and used in Eqs. (1) and (2).

$$R_c = C_u - E_{cd} - E_{ce} - C_A, \tag{1}$$

and the other for the stratiform region,

$$R_m = C_{mu} - E_{md} - E_{me} + C_A. \tag{2}$$

Leary and Houze (1980; hereafter referred to as LH) and Houze and Cheng (1981) used the above formulation to study the mass, moisture, and sensible heat fluxes associated with cloud clusters observed in GATE. They used simple models of the vertical motions and thermodynamic structures of the convective and mesoscale updrafts and downdrafts to relate the terms in (1) and (2) to the mass fluxes necessary to produce the values of those terms. Leary and Houze considered three hypothetical cases. In case A, it was assumed that neither mesoscale updraft nor downdraft existed within the mesoscale cloud system (i.e., $C_{mu} = E_{md} = 0$). In case B, a mesoscale downdraft was assumed to exist, but with no mesoscale updraft ($C_{mu} = 0$, $E_{md} > 0$), while in case C both mesoscale updraft and mesoscale downdraft were assumed to exist (C_{mu}, $E_{md} > 0$). Because of the different natures of the vertical motion and thermodynamic profiles in the convective and stratiform clouds, significantly different mass and heat fluxes were obtained for a cloud cluster, depending upon which hypothetical case was assumed.

Leary and Houze considered hypothetical cases since they were unable to determine directly several of the terms in (1) and (2) (specifically C_{mu}, E_{me}, E_{md}, E_{ce}, and C_A) because they did not have adequate data on the mesoscale available to them. However, such a data set has now been developed in the form of a composite analysis by GH. By locating wind and radar data obtained at several observation times in a coordinate system moving with a squall line (the 12 September 1974 squall line over the GATE ship array), GH were able to deduce the mesoscale air motions associated with the convective and stratiform regions of the squall system. In this study, we extend the composite analysis of GH and use it to determine a water budget based upon observations. The terms in (1) and (2) are determined empirically from the composite data fields and compared to the hypothetical budget values considered by LH.

2. The composite coordinate system and its use in this study

Gamache and Houze used radar data to determine a coordinate system moving with the leading edge of the squall line (see Fig. 2 of GH and associated discussion). Radar data for each individual observation time were then analyzed to determine which radar echoes were convective-scale echoes and which were stratiform echoes, and this information was then transferred into the moving coordinate system to determine the extent and frequency of convective and stratiform precipitation within that system (the specific criteria for determining whether a particular echo was convective or stratiform was discussed by GH and the results are shown in Figs. 4a and b of GH). Fig. 2 shows the sizes and relative locations of the regions whch GH determined to be stratiform and convective. The smaller box is the convective or "squall-line" region, while the larger box is the stratiform or "anvil" region. The cross represents the origin of the coordinate system attached to the moving squall line. The α-axis is parallel to the direction of motion of the squall line, which moved from 37° east of north, while the β-axis is perpendicular to the α-axis and represents roughly an axis parallel to the leading edge of the squall line. Henceforth, when referring to the α–β coordinate system, forward will mean the direction of motion of the squall line (negative α direction), and rearward will mean the opposite direction (positive α direction). Left will mean the negative β direction, and right will mean the positive β direction.

Gamache and Houze transferred wind data from various observation times into the α–β coordinate system and from these data determined mesoscale air motions associated with the squall system. We use the mesoscale air motions determined by GH and extend the analysis by plotting and analyzing the humidity, temperature, satellite-derived cloud brightness, and radar-derived precipitation rates in the α–

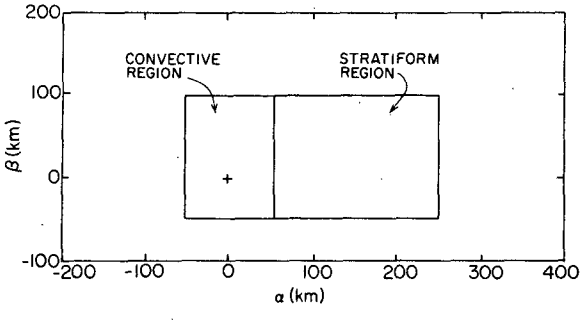

FIG. 2. The composite convective and stratiform regions as located in the α–β composite coordinate system

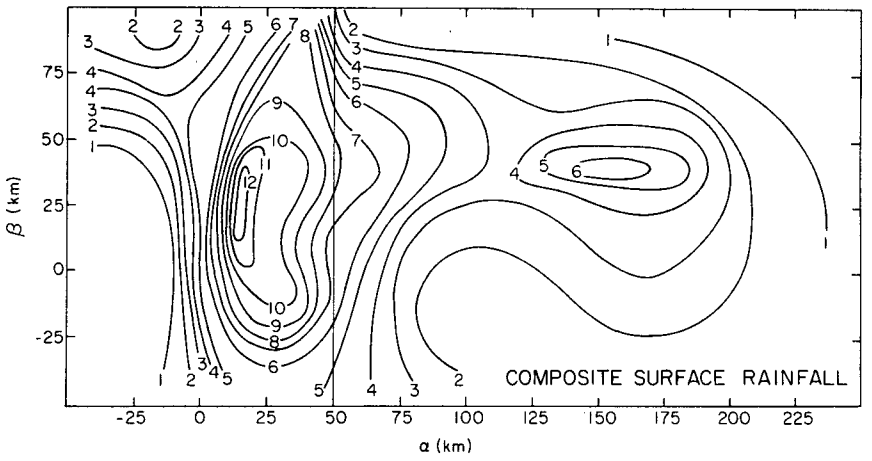

FIG. 3. Composite surface rainfall for the convective and stratiform regions as determined from hourly radar observations. Contours indicate the surface rainfall rate in mm h^{-1}.

β coordinate system. The composite mesoscale motion fields of GH, the humidity fields, and the surface radar rainfall data are then used to determine the values of all the terms in (1) and (2) except C_A, which is determined as a residual. Since C_A appears in both (1) and (2), two estimates of C_A are obtained and compared. The values of the terms in (1) and (2) are then compared to the hypothetical budget values considered by LH.

3. Data

a. Radar

In addition to the use of radar data by GH to determine the squall-line α–β coordinate system and to identify the convective and stratiform regions, we have used the radar reflectivity data to construct a composite surface-rainfall field by locating radar-determined rainfall rates at each hour from 1300 to 1800 GMT (when the squall line was detectable with the *Oceanographer* and *Researcher* shipboard radars) with respect to the α–β coordinate system and then finding the mean field of rainfall rate over the whole time period. The resulting composite surface-rainfall field is shown in Fig. 3.

The hybrid digital form of the *Oceanographer* and *Researcher* radar data[2] was used. These data are decibel values of the average radar reflectivity factor in 4 km × 4 km squares located within the range of each radar. Hudlow *et al.* (1979) discussed the bias associated with the data of each radar, when compared with raingages and other radars. They found that a correction of 2.75 dB(Z) and 2.25 db(Z) for the *Oceanographer* and *Researcher* radars, respectively, greatly reduced the discrepancies among the radar and raingage observations. They also noted the need to correct for attenuation by atmospheric oxygen and water vapor. Although this correction is actually range dependent, we simplified the procedure by adding 1.5 dB(Z) to all the data (equal to a correction for attenuation at 70 km in range). Then, the corrections were 3.75 dB(Z) for the *Researcher* and 4.25 dB(Z) for the *Oceanographer* radar. To calculate the rainfall rate R (mm h^{-1}) from the corrected radar reflectivity factor Z (mm^6 m^{-3}), we used the relationship

$$Z = 230R^{1.25}. \quad (3)$$

This relation was used by Hudlow *et al.* and is not significantly different from the refined Z–R relationship reported by Austin and Geotis (1979).

To determine the composite surface rainfall field shown in Fig. 3 the region was divided into 25 km × 25 km boxes. The values of rainfall rate in Fig. 3, particularly those in the convective region, are 25 km square averages and therefore do not reflect the real maxima in precipitation rate (~100 mm h^{-1}). The rainfall rates observed by both radars for each hour from 1300 to 1800 GMT in each 25 km × 25 km box were compared and the larger rate for that hour was accepted as the rainfall rate for that box. Assuming that beam geometry and attenuation may lead to underestimates of true rainfall rates, we choose the larger rainfall rate as the best estimate for any given situation. Since the squall line was travelling away from the *Oceanographer* and toward the *Researcher* during most of the period of the composite analysis, the *Researcher* rainfall estimates were usually higher for the leading squall line, while the *Oceanographer* rainfall estimates were usually higher for the trailing stratiform region.

To determine R_c and R_m, the rainfall-rate fields shown in Fig. 3 for the convective and stratiform

[2] Data sets No. 3.36.02.103 and 3.36.02.104, GATE Data Catalog, National Climatic Center, Asheville, North Carolina 28801.

regions were integrated over the areas of each region and these integrations were multiplied by 9 h, the period of time analyzed. The values determined for R_c and R_m were 7.2×10^{11} kg and 6.9×10^{11} kg, respectively. An alternative method would have been to sum all the rainfall associated with echoes determined to be either convective or stratiform at each observation time over the whole time period that radar data was transferred to the α–β coordinate system, regardless of whether the particular echoes were actually located within the rectangular convective or stratiform regions as displayed in Fig. 2 (see Figs. 4a and 4b of GH to see how convective precipitation at one time overlapped with stratiform precipitation at another time within the composite coordinate system). Although this method would have been more accurate in determining the actual amounts of R_c and R_m, it would have been more time consuming and the values for R_c and R_m would have been inconsistent with the time and area integrals of the composite rainfall fields for each region in Fig. 3. However, we do not believe the resulting values of R_c and R_m would be significantly different.

The surface-rainfall field for the stratiform region shown in Fig. 3, displays a rainfall rate which varied from 0.03 mm h^{-1} near β = 75 km and α = 225 km to 8 mm h^{-1} at β = 40 km and α = 50 km. The average rainfall rate in the stratiform region was 2.6 mm h^{-1}. Vertical cross sections of radar reflectivity, obtained at individual times during the period of the composite analysis and cutting through the local precipitation maximum centered at β = 40 km and α = 150 km (rainfall rate of 6 mm h^{-1}), show a well-defined radar bright band (owing to melting in a broad shallow layer), which is strong evidence that stratiform precipitation was present. The 8 mm h^{-1} maximum and 6 mm h^{-1} local maximum were both part of a band associated with and stretching rearward from intense convection located at or to the near left of the intersection of the squall line with a nearly perpendicular line of strong convection ahead of the squall line (see Fig. 3b of Shupiatsky *et al.*, 1976; Fig. 5a of GH). The 8 mm h^{-1} peak at the leading edge of the stratiform region appears to have been associated with convective cells near this intersection which were in the process of merging into the stratiform rain shield. The remainder of the band of maximum rainfall rate was probably due to the advection rearward by the relative winds from 200 to 650 mb (see Figs. 7–10 of GH) of hydrometeors produced in the intense convection near the intersection of the squall line with the convective line. As they drifted downward, the cloud and precipitation ice particles ejected from this particularly vigorous convection probably grew in the strong mesoscale updraft in the forward part of the stratiform region (see Fig. 15 of GH) and fell out along the band of maximum rainfall.

The local maximum of precipitation in the center of the stratiform region roughly coincided with the independently determined region of greatest surface divergence (Fig. 5c of GH) and the region of maximum evaporation (Fig. 11 of this article; see Section 5a), and was near the region of maximum mesoscale downdraft vertical velocity. This collocation agrees with the results of Zipser (1969) and Brown (1979), who described observational and modeling evidence that the mesoscale downdraft is maintained by cooling associated with evaporation of the stratiform rain.

b. Satellite imagery

Infrared satellite data in the form of contoured black-body radiative temperatures were used to derive the composite analysis of cloud-top temperature shown in Fig. 4. These contour plots were constructed from the gridded satellite data of Smith *et al.* (1979). Data available between 0900 and 1800 GMT were transferred into the coordinate system using the method of GH and the mean values over the composite period are shown in Fig. 4.

In most aspects, the composite satellite temperature field is consistent with the composite rainfall, vertical motion, and horizontal wind fields. It shows that there was a strong gradient from front to back in the convective region, since most of the convection occurred in the rear half of the region. Time was required for the convective cloud tops to spread out and fill in the spaces between the clouds, and in that time the relative motions carried cloud-top material toward the rear of the convective region where the minimum cloud-top temperature was 217 K corresponding to 12 km or 200 mb. The line of minimum cloud-top temperatures extended toward increasing β with increasing α and was located to the right of the secondary maximum in surface-rainfall rate. These patterns are consistent with the relative winds at 300 and 200 mb (see Figs. 9b and 10b, respectively, of GH), which evidently advected cloud ice rearward and to the right, while heavier ice particles fell out as precipitation.

Cloud-top temperatures increased from lower values at large β to higher values at low β, both in the convective and stratiform regions. This gradient of cloud-top height is in agreement with radar vertical cross sections which show that the southeastern portion of the squall line (lower β) was occupied by convection whose radar-echo tops were at only 4–5 km, much lower than the values for the center and northwestern parts of the squall line, where the tops ranged up to 16 km. In the left portion of the stratiform region, the lower cloud tops appear to be somewhat inconsistent with the vertical motion cross section (see Fig. 6 below) which shows vigorous upward motion to the rear at the 300 mb level. However, the vertical motions in the left portion of the composite

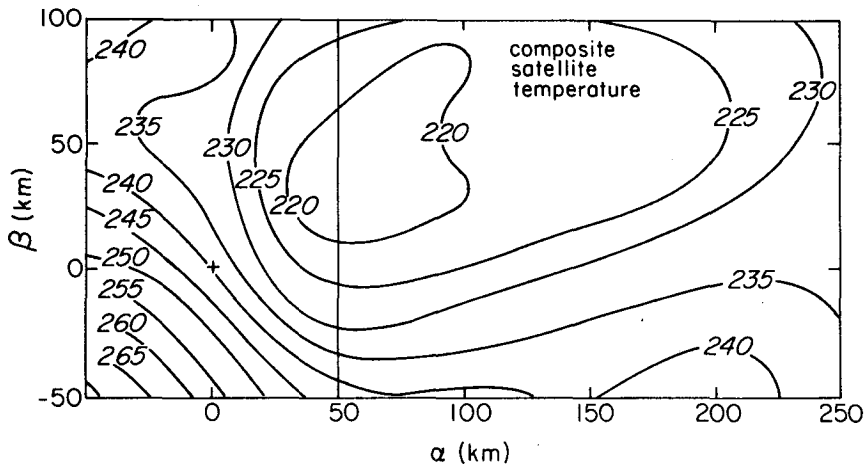

FIG. 4. Composite satellite-derived cloud-top temperatures. Contours indicate the blackbody infrared radiative temperatures (k) of clouds as observed by satellite.

analysis are more uncertain as a result of sparse wind data in that area.

c. *Horizontal wind fields*

Rawinsonde and aircraft winds were the main data sources for GH and are discussed in that article. Gamache and Houze constructed composite charts of wind data for the 9 h period from 0900 to 1800 GMT. The composite analyses were based on 150 surface observations, 50 rawinsondes and flight track winds from 3 aircraft. There were only 28 rawinsonde observations at 300 mb due to the truncation of some soundings at lower levels. Above the surface at levels without aircraft data the resolution of wind data in the squall system was between 50 and 100 km. The analyses of GH are used in this study to help determine E_{ce}, E_{me}, C_{mu}, and E_{md}.

d. *Vertical motions*

Divergence fields were calculated by GH from their composite wind charts at all analyzed levels, and average values of divergence for the convective and stratiform regions were also determined. The vertical motions given in GH have been recomputed using a cubic-spline fitting of the divergence instead of a least-squares polynomial fit. This procedure was found to decrease somewhat the value of vertical motion at cloud top. Mass balancing to obtain corrected vertical motions followed the same procedure as in GH. Results for the vertical profiles of vertical motion in the squall-line updrafts and downdrafts and the mesoscale updraft and downdraft associated with the stratiform cloud and precipitation are shown in Fig. 5. As will be described in Section 4, these region-average vertical motions will be used, together with vertical cross sections of the vertical motion, to determine the values of the water budget terms C_{mu}, E_{md}, C_u, and E_{cd}.

In GH the vertical cross sections of vertical motion shown in Fig. 15 of that paper were inadvertently described as including divergence data at 900 mb and 960 mb. Actually, the divergences at these two levels were only incorporated in the average profiles shown in Figs. 12–14 of GH. For this paper, the vertical cross sections have been recomputed using cubic

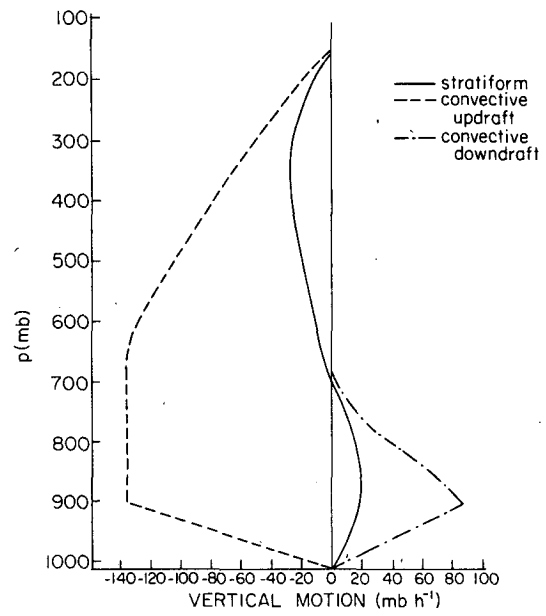

FIG. 5. Area-averaged vertical motion for the convective and stratiform regions given as pressure velocities. The solid curve indicates the average motion for the stratiform region, the dashed curve indicates the average motion in the convective region due to upward motion in convective updrafts, and the dash–dot curve indicates the average motion within the convective region due to convective downdrafts.

splines and including the divergence fields at 960 and 900 mb (Fig. 6). Owing to the much greater divergence in the left half of the stratiform region at 960 and 900 mb and the lesser divergence or convergence in the right half, the mesoscale downdraft intensity was increased in the left half of the stratiform region and decreased in the right half of the region (compare Fig. 6 with Fig. 16 of GH).

No attempt is made to account for environmental downward motion within the convective region which would be compensating the motion within the cumulonimbus and which would be near enough to the squall line for its effects to constitute a portion of the vertical profile of divergence used to calculate motions in the convective region. It is assumed that all environmental compensating downward motion occurred outside the convective region. If such compensating motion actually occurred within the convective region, the effect would probably not seriously affect our results since compensating downward motion probably was confined mainly to the upper troposphere (Fritsch and Chappel, 1980), where only a small portion of the total condensation occurred. In the lower troposphere, net motion due to the summation of all updrafts and downdrafts was smaller, and less compensating motion is therefore expected.

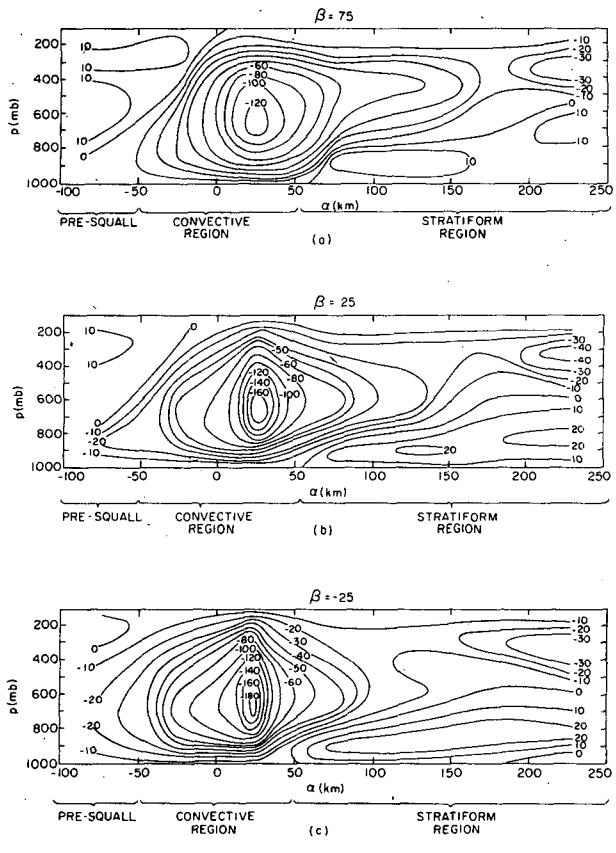

FIG. 6. Vertical cross sections of vertical motion. The contours indicate the vertical motion, given as pressure velocity, in mb h^{-1}. Cross sections are displayed in the α–p plane where (a) β = 75, (b) 25, and (c) −25 km.

e. Humidity

A composite humidity field has also been constructed in the α–β coordinate system of GH. The humidity and its horizontal and vertical gradients are needed to compute C_u, E_{cd}, C_{mu}, E_{md} and E_{ce}. The corrected humidity and temperature data derived and used by Albright *et al.* (1981) have been used in this study. The temperature data are needed to determine a value of saturation specific humidity within clouds, which tended to appear unsaturated from rawinsonde humidity data.

The data from each rawinsonde were averaged over 50 mb layers and then corrected. The correction for each rawinsonde station (in this case research ships) was constant over time, and different corrections were applied to each ship in a manner required to produce reasonable, coherent, three-dimensional mean fields of temperature and humidity for phase III of GATE.

Two cases were assumed when deriving the humidity fields within the stratiform region at 450 mb and 300 mb, where cloud evidently existed according to the composite satellite analysis (Fig. 4), the vertical motion field (Fig. 6) and the conceptual model (Fig. 1). In case I, saturation at a value halfway between ice and water saturation was assumed at 450 mb and ice saturation was assumed at 300 mb. In case II, the observed values of humidity were used at all levels. The concern associated with case II is that, at the observed temperatures, humidities were below ice saturation except toward the rear of the anvil region, which implies that cloud should not have persisted in the forward part of the stratiform region. This, however, would not be consistent with the surface rainfall pattern (Fig. 3) and the satellite composite (Fig. 4) which show high cloud tops and continuous surface rainfall in this region during the composite period. However, the fact that the regions of higher humidities tended to be correlated with the region of greater vertical motion toward the rear indicates that perhaps there was significant information in the fields of observed humidity that was not present in the humidity fields where saturation was assumed. Therefore, both cases I and II were considered.

The levels for which humidity was analyzed were the surface, 960, 900, 850, 750, 650, 450 and 300 mb. The humidity fields for these levels including case I fields for 450 and 300 mb are shown in Fig. 7 a–h. The case II fields for 450 and 300 mb are shown in Figs. 7i, j.

At the surface (Fig. 7a), a minimum in specific humidity within the stratiform region can be seen for all values of β around α = 175 km. This pattern agrees with Zipser's (1977) observation that surface specific humidity tends to reach its minimum several hours

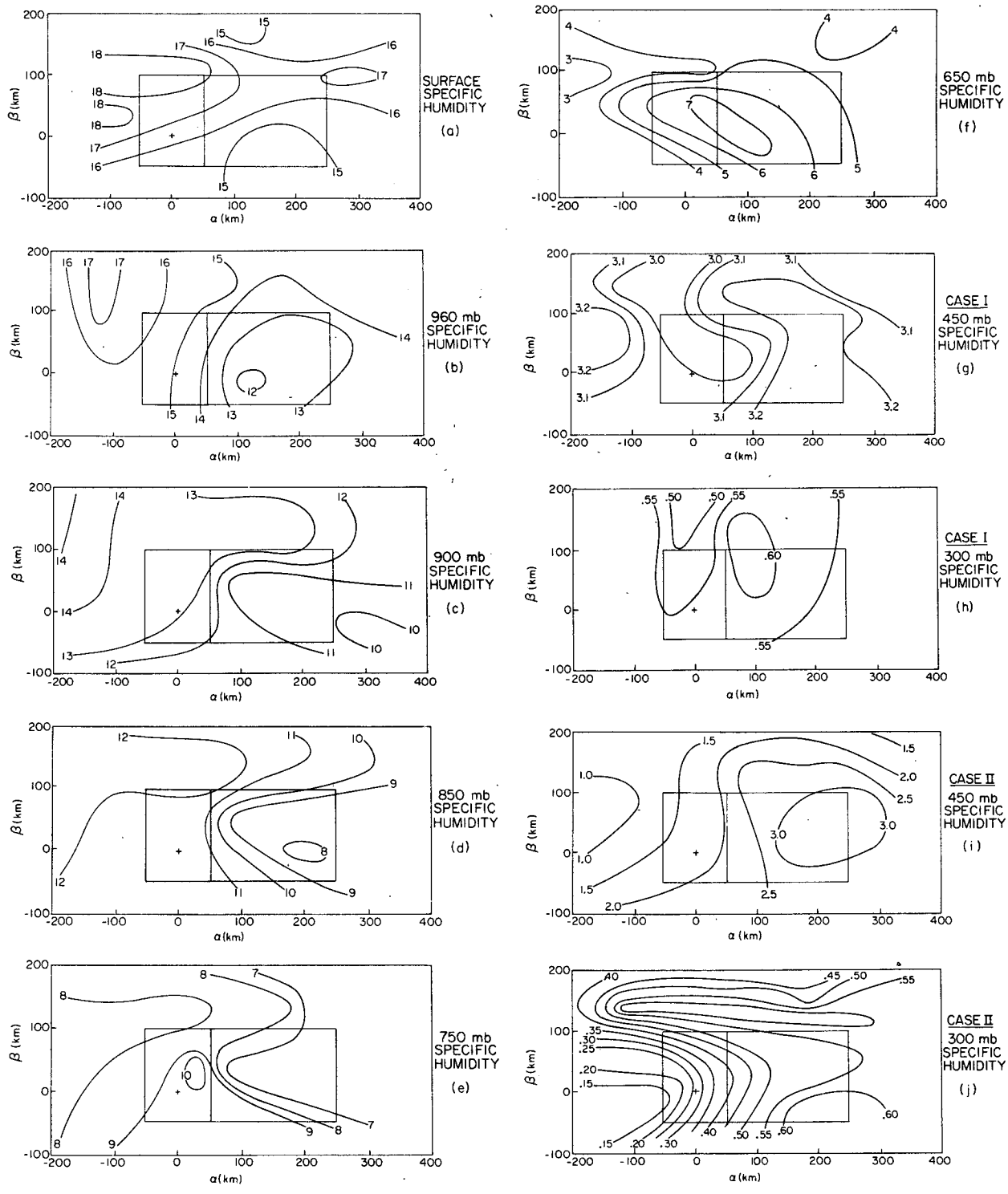

FIG. 7. Specific humidity maps. Maps are shown for (a) the surface and (b) 960 mb, (c) 900, (d) 850, (e) 750, and (f) 650 mb levels, for case I at (g) the 450 mb and (h) 300 mb levels, and for case II at (i) the 450 mb and (j) 300 mb levels. Case I and II assumptions are discussed in Section 3e. Contours show specific humidity in g kg^{-1}.

after squall line passage and lags the temperature in recovering to ambient values. The gradient of specific humidity from left to right was perhaps related to the somewhat greater rainfall rate and weaker mesoscale downdraft in the right half of the region (Figs. 3 and 6).

The humidity pattern for 960 mb (Fig. 7b) shows a minimum in the left-center portion of the stratiform region in association with the strongest downward motion, which occurred in the foreward half of the region from the surface to about 900 mb (Fig. 6). At 900, 850 and 750 mb (Figs. 7c–e), humidity decreased rapidly from the front to the rear, especially along the border between the convective and stratiform regions. In this area, the air was sinking in the mesoscale downdraft rapidly enough to counteract the effects of evaporation of rainfall (Leary, 1980). At 650 mb (Fig. 7f), this decrease was more gradual and farther to the rear, probably since the mesoscale downdraft was present at this level only toward the rear of the system (Fig. 6).

From 960 mb to 750 mb, humidity was lower in the middle of the stratiform region than on either the left or the right side. At 960 and 900 mb, the humidity was generally higher in the right half of the stratiform region, where the mesoscale downdraft was weaker, while at the 850 mb level, humidity was lowest in the center and increased approximately equally towards both the left and right borders of the region. At 750 and 650 mb, the humidity was higher in the left half of the region. This appears to have been associated with the advection of high humidity air from the convective region by the relative wind at the 750 and 650 mb levels (see Fig. 7b of GH). In the left half of the squall line region, these were important cumulus outflow levels. Radar cross sections and the satellite composite in Fig. 4 indicate that the convection was capped at about 4–5 km (immediately above the 650 mb level). At this normally dry level, strong convective outflow resulting from the forced spreading and detrainment of convective updrafts apparently increased the humidity at 650 mb, and advection by the rearward relative flow accounted for the moist tongue of air extending into the stratiform region.

At 450 and 300 mb, the humidity fields for case I (Figs. 7g, h) were nearly constant, since they simply reflected the temperature field. The case II fields (Figs. 7h, i) show increasing humidity toward the rear of the stratiform region, and saturation only near the rear; this situation was counter to the conceptual model of a tropical cloud cluster (Fig. 1), in which convective clouds blend in to the trailing stratiform cloud with no break in saturated conditions. If large quantities of water and ice (C_A) and warm saturated convective-updraft air were ejected from the convective cloud as this study suggests (Sec. 5b) and upward motion existed near the front of the stratiform region, as was found by GH, then saturation of the air flowing through the convective region into the stratiform region should have occurred rapidly. It might be suggested that one or more of the stratiform-region soundings occurred outside of the stratiform cloud. In Section 3 of GH, it is noted that the squall system was not in an absolutely steady state, and from their Fig. 4, it is apparent that the precipitation coverage was somewhat variable. However, the satellite data (Fig. 3) indicate that, even though precipitation was not reaching the ground over all the stratiform region throughout the composite period, all soundings in the stratiform region did ascend through the cloud shield. The composite of infrared satellite temperatures shown in Fig. 4 indicates that much of the cloud top was at 200–250 mb throughout the stratiform region. From the above information, we infer that case I, with saturation in the upper troposphere throughout the stratiform region, is probably the more realistic case. A probable explanation for unsaturated conditions being reported by rawinsonde is that errors occurred because the instruments became wet in the presence of cloud water, ice and saturated conditions. This error might have been particularly large in the forward part of the anvil region where vertical motion fields indicate that the cloud was deeper than in the rear part, so that the radiosonde was in cloud for an extended period.

From the foregoing discussions, it is evident that, in general, the composite radar, satellite, wind and humidity data fields constructed in GH and in the present paper for the GATE 12 September squall system are physically consistent with each other. The composite surface pressure field for this case has also been constructed by Johnson and Nicholls (1982), and it too is consistent with the other fields. This overall consistency of the composite data set lends confidence to the deductions we make from it in the remainder of this paper.

4. Determination of condensation and evaporation terms in the water budget equation

As noted in Section 3a, the convective and stratiform precipitation amounts R_c and R_m are determined from composite radar data. The term C_A in (1) and (2) is determined as a residual. The remainder of the terms which represent various forms of condensation (C_u and C_{mu}) and evaporation (E_{cd}, E_{md}, E_{ce}, E_{me}), are determined, as explained below, from the mesoscale composite wind, vertical motion and humidity fields.

a. Condensation and evaporation in convective updrafts and downdrafts

In this section, we discuss the computation of the total condensation C_u, and evaporation, E_{cd}, in convective updrafts and downdrafts, using vertical motion profiles derived from the composite vertical motion and humidity fields described in Sections 3d and e, respectively.

The values of humidity in the convective updrafts and downdrafts are derived by first assuming that all updrafts had the same thermodynamic and vertical

motion profiles and all downdrafts also had the same profiles. The value of h_c, the moist static energy within the draft, is determined for each pressure level by methods outlined below. Then assuming saturation,[3] we determine the specific humidity in the draft according to a Taylor series expansion of saturation specific humidity in terms of temperature at constant pressure [Eq. (13) of Houze *et al.* (1980)].

The value of h_c is determined under the assumptions that detrainment was zero at inflow levels and entrainment was zero at outflow levels. Since only entrainment can change h_c, the following equations are used:

$$\frac{\partial h_c}{\partial p} = \frac{1}{\omega_c}\frac{\partial \omega_c}{\partial p}(\tilde{h} - h_c), \quad \frac{\partial \omega_c}{\partial p} > 0, \tag{4}$$

$$\frac{\partial h_c}{\partial p} = 0, \quad \frac{\partial \omega_c}{\partial p} < 0. \tag{5}$$

where ω_c represents the vertical pressure-velocity of either the convective updraft or downdraft, and $\tilde{h}$ is the moist static energy of the environment. Values of $\tilde{h}$ are assumed to be the average of three soundings taken immediately in advance of the squall line. Relative winds indicate that the air sampled by these soundings was drawn into squall line updrafts and downdrafts. Eqs. (4) and (5) represent conditions of entrainment and detrainment, respectively. These equations are integrated trapezoidally in 10 mb intervals, beginning at the level of origin of either the updraft (surface) or downdraft (650 mb). For simplicity, the updrafts are assumed to have started at the ocean surface. The initial values for h_c in the updraft and downdraft are the values of $\tilde{h}$ at the surface and 650 mb, respectively. Values of ω_c are obtained from the convective updraft and downdraft profiles of Fig. 5. Convergence in the squall-line region is assumed to have been into the updrafts from the surface to 900 mb, and convergence is assumed to have fed convective downdrafts from 650 mb, the level of squall-line region non-divergence, to 900 mb (see Sec. 6c of GH). The 900 and 650 mb levels are chosen on the basis of the stability of the pre-squall soundings mentioned above. All downdraft outflow is assumed to have occurred below 900 mb.

The result of integrating (4) is a nearly constant value for moist static energy h_c in the updraft, equal to the environmental value $\tilde{h}$ at 900 mb (the inflow layer from the surface to 900 mb is rather uniform in $\tilde{h}$), since we assume no entrainment into the updraft above the 900 mb level. However, the resulting values for h_c in the downdraft change dramatically from 900 to 650 mb, since $\tilde{h}$ decreases with height rapidly and the downdraft is assumed to have entrained air from all levels in this layer. The values of humidity computed for the drafts are shown together with the mean pre-squall environment humidity in Fig. 8.

Using the values of specific humidity q, determined from h_c as described above, the vertical motions from Fig. 5 and neglecting entrainment effects, we obtain the total masses of condensation in updrafts C_u and evaporation in downdrafts E_{cd} according to

$$C_u = -\frac{A_c \tau}{g}\int_{p_T}^{p_B} \omega_{cu}(p)\frac{\partial q_u}{\partial p}\,dp, \tag{6}$$

$$E_{cd} = \frac{A_c \tau}{g}\int_{p_{TD}}^{p_s} \omega_{cd}(p)\frac{\partial q_d}{\partial p}\,dp, \tag{7}$$

where q_u and q_d are the specific humidities in the convective updrafts and downdrafts, respectively, A_c is the area of the convective region rectangle (Fig. 2), τ is the 9 h period of the composite, p_B is the pressure at cloud base (950 mb), p_T is the pressure at the top of the updraft (150 mb), P_{TD} is the pressure at the top of the downdraft (650 mb), p_s is surface pressure (1014 mb), g is the gravitational acceleration, and ω_{cu} and ω_{cd} are the pressure-velocities for the squall line updrafts and downdrafts, respectively. In general,

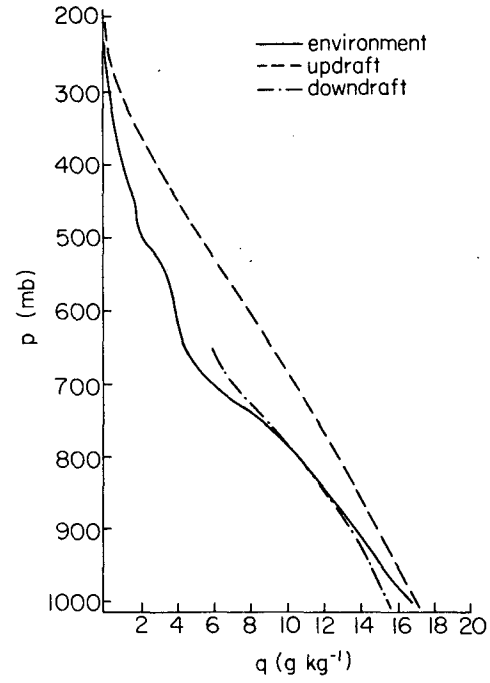

FIG. 8. Vertical profiles of specific humidity used in the calculations of C_u and E_{cd} (see Section 4a). The solid curve shows the values of humidity in the pre-squall environment, which supplies most of the inflow into the convective region, the dashed line shows the profile computed for the convective updrafts in the squall line and the dash–dot curve shows the profile computed for the convective down-drafts in the squall line.

[3] Zipser (1977) studied several tropical squall systems and found cold, nearly saturated air near the surface which was attributable to convective downdrafts.

an entrainment term should appear in the integrands of (6) and (7) [see Eqs. (29) and (39) of Houze *et al.* (1980)]. However, the entrainment term in (6) is zero by the assumptions we have made, except between p_B (=950 mb) and 900 mb, and therefore has a negligible effect. In (7) the entrainment term can be neglected since the environment and downdraft values of q are nearly the same (Fig. 8). Eqs. (6) and (7) are integrated trapezoidally from p_T to p_B and p_{TD} to p_s, respectively, in 50 mb intervals, and $\partial q_u/\partial p$ and $\partial q_d/\partial p$ are calculated by centered differencing using 50 mb intervals of q.

b. *Computation of stratiform condensation and evaporation*

To compute the condensation C_{mu} that occurs in the stratiform cloud and the evaporation E_{md} that occurs below the base of the cloud, the stratiform box (Fig. 2) is subdivided into 50 km × 50 km horizontal grid squares. Each grid square defines a vertical column within which condensation and evaporation are obtained by integrating vertically. Then the values of C_{mu} and E_{md} are obtained by adding the results for all the vertical columns. This procedure allows the horizontal variation of the height of the base of the stratiform cloud to be taken into account.

The condensation and evaporation in each grid column are determined from the water continuity equation

$$\frac{dq}{dt} = e - c, \tag{8}$$

where e is evaporation and c is condensation. Application of the chain rule of partial differentiation and averaging horizontally over a grid column allows (8) to be rewritten as

$$\frac{\partial \bar{q}}{\partial t} + \bar{\omega}\frac{\partial \bar{q}}{\partial p} + \bar{\mathbf{V}}_r \cdot \nabla \bar{q} + \overline{\omega' \frac{\partial q'}{\partial p}} + \overline{\mathbf{V}_r' \cdot \nabla q'} = \bar{e} - \bar{c}, \tag{9}$$

where $\mathbf{V}_r$ is the horizontal wind relative to the motion of the squall line. The barred quantities represent averages over a grid square. The primed quantities are deviations from these averages and are involved in turbulent-flux terms. Humidity and winds in the convective and stratiform regions are assumed to have been in a steady state following the motion of the squall system. Hence, in the coordinate frame moving within the system,

$$\frac{\partial \bar{q}}{\partial t} = 0. \tag{10}$$

Then, neglecting turbulent fluxes, we obtain for the stratiform region

$$\bar{\omega}\frac{\partial \bar{q}}{\partial p} + \bar{\mathbf{V}}_r \cdot \nabla \bar{q} = \bar{e} - \bar{c}. \tag{11}$$

This equation is used at all levels. Since at 960 mb and at the surface, i.e. within the boundary layer, neglect of turbulent fluxes is not justified, diagnosed values of $\bar{e} - \bar{c}$ at these levels must therefore be interpreted carefully (see discussion in Section 5a). To evaluate $\bar{e} - \bar{c}$, values of $\bar{q}$ are obtained from Figs. 7a–j at all grid points where α = 50, 100, 150, 200 or 250 km, and β = −50, 0, 50 or 100 km.

The vertical air motions illustrated in Fig. 6 are used to determine the value of ω in (11). The values of ω are obtained at α = 75, 125, 175 and 225 km and β = −25, 25 and 75 km. Values of humidity and its gradients for these points are obtained from

$$\bar{q}(\alpha, \beta) = [\bar{q}(\alpha + \Delta\alpha, \beta + \Delta\beta) + \bar{q}(\alpha + \Delta\alpha, \beta - \Delta\beta) + \bar{q}(\alpha - \Delta\alpha, \beta + \Delta\beta) + \bar{q}(\alpha - \Delta\alpha, \beta - \Delta\beta)]/4, \tag{12}$$

$$\frac{\partial \bar{q}}{\partial \alpha} = [\bar{q}(\alpha + \Delta\alpha, \beta + \Delta\beta) + \bar{q}(\alpha + \Delta\alpha, \beta - \Delta\beta) - \bar{q}(\alpha - \Delta\alpha, \beta + \Delta\beta) - \bar{q}(\alpha - \Delta\alpha, \beta - \Delta\beta)]/4\Delta\alpha, \tag{13}$$

$$\frac{\partial \bar{q}}{\partial \beta} = [\bar{q}(\alpha + \Delta\alpha, \beta + \Delta\beta) + \bar{q}(\alpha - \Delta\alpha, \beta + \Delta\beta) - \bar{q}(\alpha + \Delta\alpha, \beta - \Delta\beta) - \bar{q}(\alpha - \Delta\alpha, \beta - \Delta\beta)]/4\Delta\beta, \tag{14}$$

where $\Delta\alpha$ and $\Delta\beta$ = 25 km. The values of $\bar{q}$ and $\bar{\mathbf{V}}_r \cdot \nabla\bar{q}$ are then fitted in the vertical with respect to pressure using a cubic-spline interpolation for each grid column. Vertical derivatives of $\bar{q}$ are obtained using the spline coefficients. Vertical cross sections, at β = 75, 25, and −25 km, of the fitted values of $\bar{\omega}\partial\bar{q}/\partial p$, $\bar{\mathbf{V}}_r \cdot \nabla\bar{q}$, and $\bar{e} - \bar{c}$ are shown in Figs. 9–11, respectively. These figures will be discussed in Section 5a.

The composite fields of $\bar{e} - \bar{c}$ are integrated vertically (using a trapezoidal integration with a 50 mb interval) in each 50 km × 50 km grid column and then all grid columns are summed to obtain the bulk values of C_{mu} and E_{md} as follows

$$C_{\mathrm{mu}} = -\frac{\tau}{g}\int_{A_s}\int\int_{p_{Ts}}^{p_m} (\bar{e} - \bar{c})\,dp\,dA, \tag{15}$$

$$E_{md} = \frac{\tau}{g}\int_{A_s}\int\int_{p_m}^{p_s} (\bar{e} - \bar{c})\,dp\,dA, \tag{16}$$

where A_s is the area of the stratiform-region rectangle, P_{Ts} refers to the top of the stratiform cloud (150 mb), p_s the surface pressure (1014 mb) and p_m is cloud base, defined here as the pressure level where $\bar{e} - \bar{c}$ changes sign. This level corresponds roughly to the height where $\bar{\omega} = 0$.

c. Calculation of evaporation of condensate in environmental air

Evaporation of convective cell condensate into environmental air (E_{ce}) is assumed to have occurred as air flowed horizontally through the convective region from front to rear. Condensate ejected from the tops of convective cells is assumed to have evaporated into this environmental air as it passed through the convective region and around the convective towers. Another important factor in modifying the humidity of the air passing through the region was the ejection of saturated air from cumulus cells. Water vapor diverging from convective updrafts and downdrafts constituted vapor added to the air in the environment of the cells, while water vapor converging into convective drafts was vapor that was removed from the air passing around the cells.

The evaporation in the environment E_{ce} should not be confused with the evaporation E_{cd} occurring within the convective cells [recall Eq. (1)]. To compute E_{ce}, we have to specify the region to be considered as the environment of the cells. We assume here that the evaporation in the environment occurs within the convective region but outside the cells; that is, the environment region consists of the convective region (defined in Fig. 2) minus the areas covered by active cells. The net inflow (outflow) of water vapor into (from) this environment region is the sum of vapor flowing into (out of) the convective region across the outer boundary of the convective region and the vapor flowing out of (into) the convective drafts and thence into (out of) the convective region. The total mass of water vapor entering the region is thus given by

$$Q_{\text{in}} = -\frac{\tau}{g}\int_{p_T}^{650\text{ mb}}\oint_{l_B}\delta_{\text{in}}\bar{q}_B\bar{\mathbf{V}}_{rB}\cdot d\mathbf{n}dp + \frac{A_c\tau}{g}\int_{p_T}^{650\text{ mb}} q_u(\nabla\cdot\bar{\mathbf{V}}_r)_u dp, \quad (17)$$

and the total mass of water vapor leaving the region is given by

$$Q_{\text{out}} = \frac{\tau}{g}\int_{p_T}^{650\text{ mb}}\oint_{l_B}\delta_{\text{out}}\bar{q}_B\bar{\mathbf{V}}_{rB}\cdot d\mathbf{n}dp. \quad (18)$$

Q_{in} and Q_{out} represent the total masses of water vapor transported into and out of the environment region above 650 mb, δ_{out} is set to one for outflow and zero for inflow, and δ_{in} is set to one for inflow and zero for outflow. The value of specific humidity along the border of the convective region is given by $\bar{q}_B$, l_B is the border of the convective region, $\mathbf{n}$ is the unit vector normal to l_B, and $\bar{\mathbf{V}}_{rB}$ is the horizontal relative wind at the boundary of the convective region. The subscript u refers to the convective updraft. The first term in both (17) and (18) represents the advection of humidity across the outside border of the convective region. The second term in (17) represents the outflow of water vapor from convective updrafts into the environment region. The 650 mb level was chosen as the boundary of the integration because it is the lowest level of updraft outflow and therefore the lowest level at which cloud water and ice are expelled from the cumulonimbus. Vertical advection of water vapor through the 650 mb level need not be considered since the vertical motion outside the convective drafts is assumed to be zero. Eqs. (17) and (18) are integrated trapezoidally from one analyzed level to the next. Grid point values of $\bar{q}_B$ (from the analyses in Fig. 7) and $\mathbf{V}_r$ (from the analyses in GH) are determined around the border of the convective region at 50 km intervals.

The amount of evaporation E_{ce} is the difference between Q_{out} and Q_{in}, i.e.,

$$E_{ce} = Q_{\text{out}} - Q_{\text{in}}. \quad (19)$$

Values of E_{ce} are determined under the two assumptions discussed in Section 3e.

The evaporation of stratiform cloud into the squall-system environment (E_{me}) is determined by computing the total outflow of the relative horizontal winds from the stratiform region and assuming a hydrometeor concentration of q_{lm} = 0.5 g/kg (see footnote 4). Thus the amount of water that leaves the stratiform cloud to evaporate in the large-scale environment is given by

$$E_{me} = \frac{\tau}{g}\int_{p_{Ts}}^{p_m}\oint_{l_B} q_{lm}\delta_{\text{out}}\bar{\mathbf{V}}_r\cdot d\mathbf{n}dp, \quad (20)$$

where l_B is the boundary of the stratiform region. This expression is integrated trapezoidally from one analyzed level to the next, and interpolated grid point values of $\bar{\mathbf{V}}_r$ at 50 km intervals are used to determine the line integral.

5. Results

a. Cross sections of evaporation and condensation in the stratiform region

Cross sections of evaporation minus condensation ($\bar{e} - \bar{c}$) and the terms contributing to its calculation according to (11) are shown in Figs. 9–11. The horizontal advection term $\bar{\mathbf{V}}_r\cdot\nabla\bar{q}$ (Fig. 9) is considerably smaller that the vertical advection term $\bar{\omega}\partial\bar{q}/\partial p$ (Fig. 10) everywhere except in the region of the mesoscale updraft (Fig. 6) in case II (the unsaturated or observed

[4] This value of q_{lm} is consistent with the work of Churchill (1982), in which the hydrometeor mixing ratio indicated by radar was approximately 0.5 g kg^{-1} at several mid-to-upper tropospheric levels in cloud clusters observed in the Winter Monsoon Experiment (MONEX).

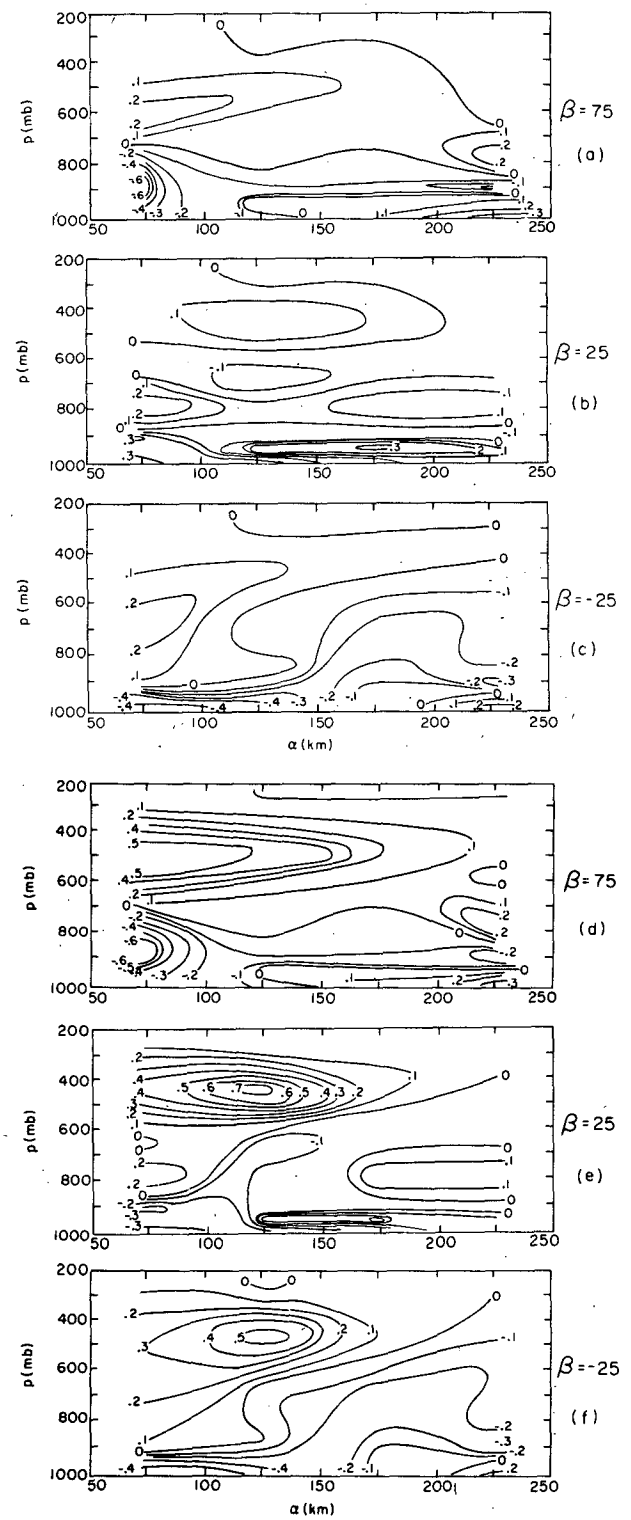

FIG. 9. Vertical cross sections of $\bar{\mathbf{V}}_r \cdot \nabla \bar{q}$. Case I cross sections in the α–p plane are shown for (a) $\beta = 75$, (b) 25, and (c) -25 km, and case II cross sections in the α-p plane are shown for (d) $\beta = 75$, (e) 25, and (f) -25 km. Contours are in g kg^{-1} h^{-1} (see Section 4b).

humidity case). The larger value of $\bar{\mathbf{V}}_r \cdot \nabla \bar{q}$ in case II would have to be explained by continuing evaporation of water and ice ejected from squall line updrafts after that water had left the convective region (recall

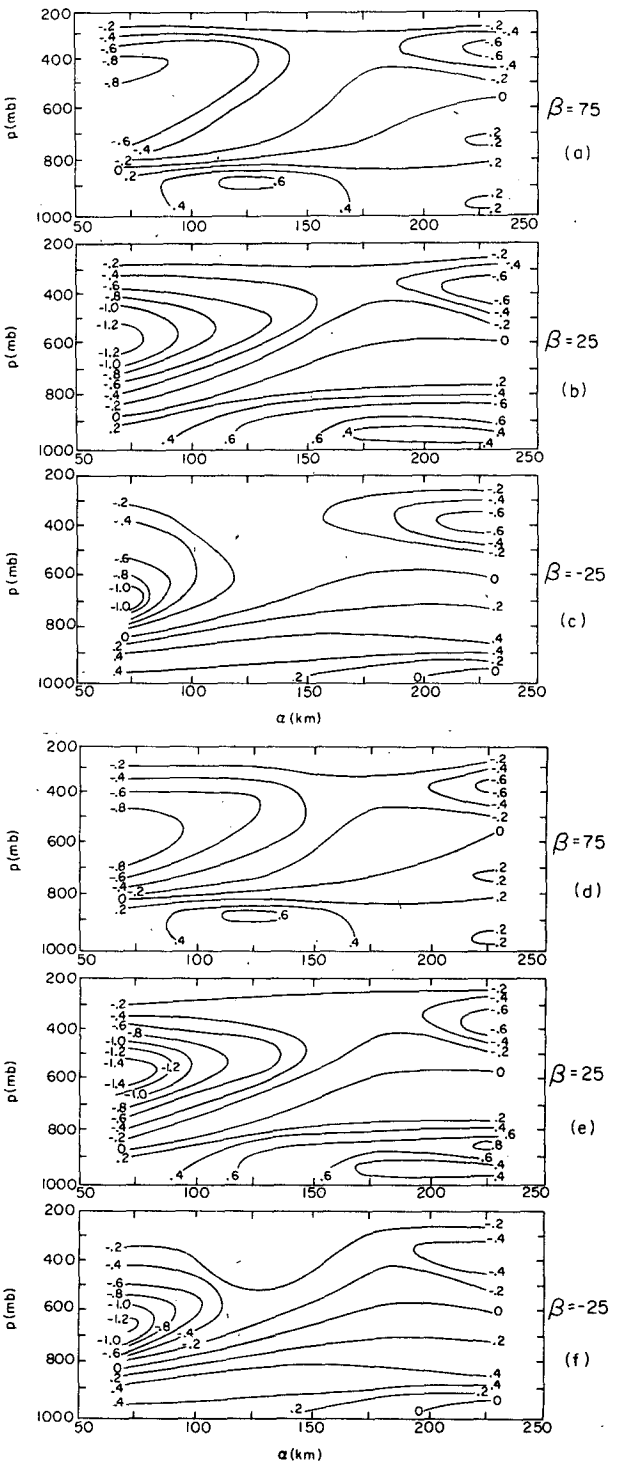

FIG. 10. As in Fig. 9 except for $\bar{\omega}\partial\bar{q}/\partial p$ (see Section 4b).

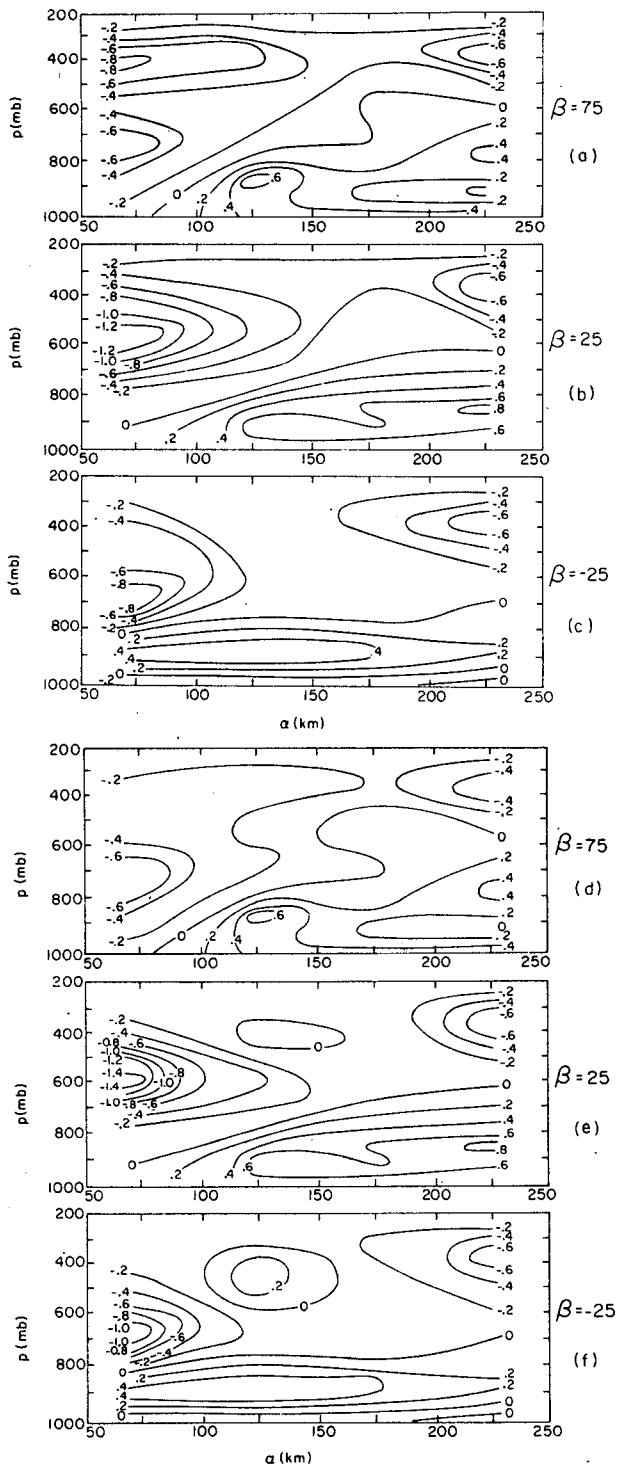

FIG. 11. As in Fig. 9 except for evaporation minus condensation ($\bar{e} - \bar{c}$) (see Section 4b).

the horizontal gradient of $\bar{q}$ in Fig. 7j compared to Fig. 7h and that the relative flow at this level seen in Fig. 9b of GH, was from front to rear in the system). This slow process of evaporation is reflected further in a smaller value of E_{ce} in case II (see Section 5b), the difference from case I being that part of the evaporation is assumed to have occurred in the stratiform region.

As expected, the general configuration of $\bar{e} - \bar{c}$ (Fig. 11) shows evaporation in the lower troposphere, within the mesoscale downdraft, and condensation in the upper troposphere, within the mesoscale updraft. The border between condensation and evaporation (i.e., the stratiform cloud base) sloped upward toward the rear of the stratiform region. This slope was associated primarily with the upward slope of the border between updraft and downdraft, although the border was altered somewhat by the horizontal advection term $\bar{V}_r \cdot \nabla \bar{q}$. Condensation is indicated to have been greatest in the forward part of the stratiform region, particularly along $\beta = 25$, where the strongest upward vertical motion was present, decreased from there to $\alpha = 175$ km and then increased toward the rear of the stratiform region, resulting in a secondary maximum in condensation, which corresponded in location to a secondary maximum in upward air motion seen in Fig. 6 and discussed by GH. The condensation in the forward part of the stratiform region evidently contributed to the stratiform precipitation area seen in Fig. 3, while the condensation at the rear of the region contributed to the extension of the stratiform cloud (Fig. 4) beyond the stratiform region rainfall. The condensate produced there eventually evaporated in the large-scale environment with little or none reaching the surface as rain. Maximum evaporation within the stratiform region occurred generally between 850 and 950 mb in the warm unsaturated air within the lower mesoscale downdraft. As noted in Section 3a, this maximum of evaporation (near $\alpha = 125$, $\beta = 25$ km in Fig. 11b) was roughly collocated with the maximum mesoscale downdraft (Fig. 6; $\alpha = 125$ km, $\beta = -25$ km) and the surface stratiform rainfall maximum at $\alpha = 160$ km and $\beta = 30$ km in Fig. 3. Evaporation was somewhat less along $\beta = 75$ km (Fig. 11a) and much less along $\beta = -25$ km (Fig. 11c). Along $\beta = -25$ km, condensation diagnosed near the surface may have been partly a result of neglecting the turbulent mixing in Eq. (11). In this region of diagnosed condensation, there was strong vertical shear of the horizontal wind, but low surface wind velocity. For example, at $\beta = 0$ km and $\alpha = 100$ km, the surface relative wind velocity was 5 m s^{-1} from 63° while at 850 mb the velocity was 20 m s^{-1} from 99°. Zipser (1977) noted that in regions of strong shear but low surface wind velocities, the air in the boundary layer may be dried more by the entrainment downward into the boundary layer of dry mesoscale-downdraft air than it is moistened by evaporation from the sea surface. If this type of drying occurs, it is improperly

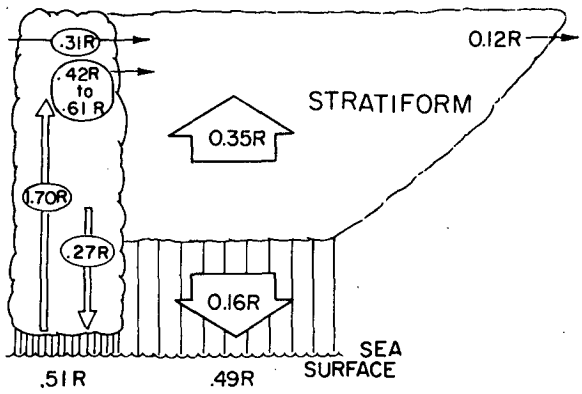

FIG. 12. Schematic diagram of the squall-system water budget as in Fig. 1, except the budget variables have been replaced with their values as determined in this study. Values are expressed as fractions of the total rainfall ($R_m + R_c$).

diagnosed as condensation (which also lowers specific humidity) by Eq. (11).

Uncertainties in the humidity measurements and in the determination of $\bar{\omega}$ make the details of the spatial variations of the $\bar{\mathbf{V}}_r \cdot \nabla\bar{q}$, $\bar{\omega}\partial\bar{q}/\partial p$ *and* $\bar{e} - \bar{c}$ seen in Figs. 9–11 somewhat uncertain; however, the volume integrals of these quantities used in the determination of the bulk stratiform condensation C_{mu} and evaporation E_{md} [Eqs. (15) and (16)] should be more accurate.

b. *Water budget parameters*

The water budget parameters C_u, E_{cd}, E_{ce}, C_{mu}, E_{me} and E_{md} [Fig. 1; Eqs. (1) and (2)] have been determined from the composite wind and thermodynamic data discussed in this paper and in GH using the methods discussed in Section 4 of this paper. Radar data have been used (in Section 3) to determine R_c and R_m. Finally, C_A has been determined as a residual in both (1) and (2). The values obtained for these parameters are summarized in Fig. 12 and Tables 1 and 2.

TABLE 1. Values of the components of the water budget of a mesoscale convective system for cases A, B and C of Leary and Houze (1980, LH) and cases I and II of the present study. Numbers in each case are expressed as fractions of the total rain ($R_c + R_m$).

Case	R_c =	C_u	$-E_{cd}$	$-E_{ce}$	$-C_A$
LH-A	0.60	1.30	−0.17	−0.09	−0.44
LH-B	0.60	1.75	−0.23	−0.12	−0.80
LH-C	0.60	1.25	−0.16	−0.09	−0.40
I	0.51	1.70	−0.27	−0.31	−0.61
II	0.51	1.70	−0.27	−0.05	−0.87
Case	R_m =	C_{mu}	$-E_{md}$	$-E_{me}$	$+C_A$
LH-A	0.40	0	−0	−0.04	+0.44
LH-B	0.40	0	−0.32	−0.08	+0.80
LH-C	0.40	0.40	−0.32	−0.08	+0.40
I	0.49	0.35	−0.16	−0.12	+0.42
II	0.49	0.26	−0.16	−0.12	+0.51

TABLE 2. Contributions of C_{mu} and C_A to total condensate of the stratiform anvil cloud. Contributions are expressed as fractions of the total condensate.

Ratio	LH-C	I	II
$\frac{C_{mu}}{C_{mu} + C_A}$	0.50	0.41	0.26
$\frac{C_A}{C_{mu} + C_A}$	0.50	0.59	0.74

In Table 1, the results of this study are compared to the water budgets considered by LH. The numbers in the table indicate the relative sizes of the different parameters as a fraction of the total rainfall R (the sum of R_c and R_m) which in our case is 14.1×10^{11} kg. On the basis of results of Houze (1977) and Cheng and Houze (1979), LH assumed values of 0.60 and 0.40 for R_c/R and R_m/R, respectively, to represent a typical GATE mesoscale convective system. In our case, R_c/R is found to be 0.51 and R_m/R is 0.49. These values are not significantly different from the typical GATE values.

In case A of LH, it was assumed that the stratiform rain was produced without any mesoscale updraft or downdraft motion. Hence C_{mu} and E_{md} were both set equal to zero. Condensation could then only occur in the updrafts of convective cells (C_u), and the only way to explain the stratiform precipitation was via a large transfer (C_A) of condensate from the cells into the stratiform cloud. Thus, C_A nearly matched R_m in case A.

In case B, it was assumed that there was no mesoscale updraft in the stratiform cloud but that there was a substantial mesoscale downdraft. Thus, again, the convective cells had to provide the condensate for the entire mesoscale system. Moreover, since enough condensate had to be supplied to the stratiform cloud not only to explain the observed stratiform rain (R_m) but also to account for the water evaporated in the mesoscale downdraft (E_{md}), the amount of condensation in cells (C_u) and the transfer of condensate from cells to stratiform cloud (C_A) had to be greater than in case A.

In case C, it was assumed that the stratiform region of the mesoscale system had both a strong mesoscale downdraft and a well developed mesoscale updraft. In this case, some condensation (C_{mu}) occurred in the mesoscale updraft within the stratiform region itself. Therefore, the stratiform precipitation (R_m) and mesoscale downdraft evaporation did not have to be supplied entirely by transfer of condensate from cells (C_A). Hence C_u and C_A were smaller in case C than in case A. Case C was devised by LH such that mesoscale updraft condensation in the stratiform cloud

(C_{mu}) and transfer of condensate into the stratiform region from cells (C_A) contributed equally as sources of stratiform cloud water (Table 1 shows $C_{mu} = C_A$ in case C). In this respect, case C of LH resembles Brown's (1979) numerical model simulation of a tropical squall line in which also roughly half (44%) of the stratiform cloud water was produced by mesoscale updraft condensation.

Our calculations for the GATE 12 September squall line system (cases I and II in Table 1) show a water budget similar to case C of LH [their case with both mesoscale updraft and downdraft (LH-C)] except for E_{md}, which is half of the 0.32 of LH-C, and E_{ce}, which at 0.31 for case I is three times that of LH-C. The higher value for E_{ce} is due to the consideration of the strong flow through the squall line at upper levels and the case I assumption that the air was saturated upon leaving the squall line region. Except for comparisons involving E_{md} and E_{ce}, all the terms in LH-C and our cases I and II are within a factor of two. The primary difference in our results and those of LH-C is in the relative magnitudes of C_{mu} and C_A. Since the total water supplied to the stratiform anvil cloud is $C_{mu} + C_A$, the ratios $C_{mu}/(C_{mu} + C_A)$ and $C_A/(C_{mu} + C_A)$ indicate the contributions of mesoscale updraft condensation and incorporation of condensate from convective cells to the make-up of the stratiform cloud. These ratios are indicated in Table 2 for the three cases. In LH-C, the sources were arbitrarily set each to contribute 0.50 of the total condensate. This result indicated the substantial importance of the mesoscale updraft as a source of anvil condensate. Our results for the 12 September GATE squall line system, indicate again that the mesoscale updraft was an important source of condensate for the stratiform cloud, contributing 0.26–0.41 of the total.

This result, however, implies that the transfer from the convective cells (C_A), which contributed the remaining 0.59–0.74 of the anvil condensate, was the more important source. Yet this transfer is the least understood process in the water budget; in this study, the term C_A has been computed as the residual of all the other processes (C_u, E_{cd}, R_c, E_{ce}, C_{mu}, E_{me}, E_{md} and R_m). Future work should be directed toward elucidating the physical mechanisms by which the transfer is made. Houze (1981) suggested that ice particles in the upper regions of cumulonimbus towers in the convective region fall so slowly that they are displaced by a large horizontal distance from the convective region before they melt and fall to the surface as rain. Houze and Smull (1982) and Chen and Zipser (1982) suggested further that this horizontal displacement of ice particles may be enhanced by the relative wind at mid-levels in mesoscale convective systems. Strong relative flow directed toward the stratiform region from the convective region at the 450 mb level in the GATE 12 September squall system (Fig. 8b of GH) indicates that such a process was occurring in our case. Further work on the trajectories of ice particles in mesoscale systems is needed to evaluate quantitatively the importance of the horizontal displacement of ice particles from the tops of convective cells in contributing to C_A. Understanding of other processes that may contribute to C_A should also be sought, and C_A should be computed from physical principles and observations instead of as a residual term.

6. Conclusions

The water budget of a mesoscale convective system in the tropics has been determined from composite fields of horizontal wind, vertical motion, humidity and precipitation data for a GATE squall line cloud cluster. In most respects, the water budget determined from these data resembles the water budget hypothesized to be realistic for such systems by LH. Forty-nine percent of the rain falling from the system was stratiform, and condensation in the mesoscale updraft of the stratiform anvil cloud (C_{mu}) contributed significantly to the production of the stratiform rain. However, our data show that C_{mu} accounted for only 25–40% of the total condensate making up the stratiform anvil cloud, a somewhat smaller fraction than suggested by LH. The remaining 60–75% of the stratiform cloud was created by the horizontal transfer of condensate from convective towers into the stratiform region of the cloud system (C_A). Thus, C_A was the larger source of stratiform condensate in our case. However, the mechanism of this horizontal transfer of condensate is the least well understood aspect of the water budget; in this study, C_A has been computed as a residual of the other components of the water budget. Therefore, future efforts should be directed toward the intensive study of the fallout and growth of ice particles in the circulation pattern of a tropical mesoscale convective system. Understanding gained from such studies should allow the determination of C_A from physical principles and observations rather than as a residual quantity.

Acknowledgments. The authors are grateful to M. D. Albright, S. D. Bell, S. K. Esbensen and E. E. Recker for advice and help in processing the data for the composite analyses. This research has been supported by the Global Atmospheric Research Program, Division of Atmospheric Sciences, National Science Foundation, under Grant ATM80-17327.

REFERENCES

Albright, M. D., D. R. Mock, E. E. Recker and R. J. Reed, 1981: A diagnostic study of the diurnal rainfall variation in the GATE B-scale area. *J. Atmos. Sci.*, **38**, 1429–1435.

Austin, P. M., and S. G. Geotis, 1979: Raindrop sizes and related parameters for GATE, *J. Appl. Meteor.*, **18**, 569–575.

Brown, J. M., 1979: Mesoscale unsaturated downdrafts driven by rainfall evaporation: A numerical study. *J. Atmos. Sci.*, **36**, 313–338.

Chen, Y.-L., and E. J. Zipser, 1982: The role of horizontal advection of hydrometeors in the water budget of a large squall line system. *Preprints 12th Conf. Severe Local Storms,* San Antonio, Amer. Meteor. Soc., 335–358.

Cheng, C.-P., and R. A. Houze, Jr., 1979: The distribution of convective and mesoscale precipitation in GATE radar echo patterns. *Mon. Wea. Rev.*, **107**, 1370–1381.

Churchill, D. D., 1982: Development and structure of winter monsoon cloud clusters. M.S. thesis, University of Washington, 223 pp.

Frank, N. L., 1970: Atlantic tropical systems of 1969. *Mon. Wea. Rev.*, **98**, 307–314.

Fritsch, J. M., and C. F. Chappell, 1980: Numerical prediction of convectively driven mesoscale pressure systems. Part II: Mesoscale model. *J. Atmos. Sci.*, **37**, 1734–1762.

Gamache, J. F., and R. A. Houze, Jr., 1982: Mesoscale air motions associated with a tropical squall line. *Mon. Wea. Rev.*, **110**, 118–135.

Houze, R. A., Jr., 1977: Structure and dynamics of a tropical squall-line system. *Mon. Wea. Rev.*, **105**, 1540–1567.

——, 1981: Structure of atmospheric precipitation systems—A global survey. *Radio Sci.*, **16**, 671–689.

——, 1982: Cloud clusters and large-scale vertical motions in the tropics. *J. Meteor. Soc. Jpn,* **60**, 396–409.

——, and A. K. Betts, 1981: Convection in GATE. *Rev. Geophys. Space Phys.*, **16**, 541–576.

——, and C.-P. Cheng, 1981: Inclusion of mesoscale updrafts and downdrafts in computations of vertical fluxes by ensembles of tropical clouds. *J. Atmos. Sci.*, **38**, 1751–1770.

——, and P. V. Hobbs, 1982: Organization and structure of precipitating cloud systems. *Advances in Geophysics,* Vol. 24, Academic Press. 225–315.

——, and B. F. Smull, 1982: Comparison of an Oklahoma squall line to mesoscale convective systems in the tropics. *Preprints, 12th Conf. Severe Local Storms,* San Antonio, Amer. Meteor. Soc., 338–341.

——, C.-P. Cheng. C. A. Leary, and J. F. Gamache, 1980: Diagnosis of cloud mass and heat fluxes from radar and synoptic data. *J. Atmos. Sci.*, **37**, 754–773.

Hudlow, M. D., 1979: Mean rainfall patterns for the three phases of GATE. *J. Appl. Meteor.*, **18**, 1656–1669.

——, V. Patterson, P. Pytlowany, F. Richards and S. Geotis, 1979: Calibration and intercomparison of the GATE C-band weather radars. NOAA Tech. Rep. EDIS 31, 98 pp. Center for Environmental Assessment Services. [NTIS PB8120305.]

Johnson, R. H., and M. E. Nicholls, 1982: A composite analysis of the boundary layer accompanying a tropical squall line. *Mon. Wea. Rev.*, **111**, 308–319.

Leary, C. A., 1980: Temperature and humidity profiles in mesoscale unsaturated downdrafts. *J. Atmos. Sci.*, **37**, 1005–1012.

——, and R. A. Houze, Jr., 1980: The contribution of mesoscale motions to the mass and heat fluxes of an intense tropical convective system. *J. Atmos. Sci.*, **37**, 784–796.

Maddox, R. A., 1980: Mesoscale convective complexes. *Bull. Amer. Meteor. Soc.*, **61**, 1374–1387.

——, 1981: The structure and life cycle of mid-latitude mesoscale convective complexes. Atmos. Sci. Pap. No. 336, Colorado State University, 331 pp.

Martin, D. W., and V. E. Suomi, 1972: A satellite study of cloud clusters over the tropical North Atlantic Ocean, *Bull. Amer. Meteor. Soc.*, **53**, 135–156.

Shupiatsky, A. B., G. N. Evseonok and A. I. Korotov, 1976: Investigation of clouds in the ITCZ with satellite and ship radar. *TROPEX-74,* Vol. 1, *Atmosphere,* Gidrometeorizdat, Leningrad, 515–520. [in Russian]

Smith, E. A., T. H. Vonder Haar, and M. Whitcomb, 1979: GATE Satellite surface radiation data archives. Tech. Rep. Dept. Atmos. Sci., Colorado State University, 210 pp.

Zipser, E. J., 1969: The role of organized unsaturated convective downdrafts in the structure and rapid decay of an equatorial disturbance. *J. Appl. Meteor.*, **8**, 799–814.

——, 1977: Mesoscale and convective-scale downdrafts as distinct components of squall-line circulation. *Mon. Wea. Rev.*, **105**, 1568–1569.